Journal of Vibration Engineering & Technologies (2022) 10:1905–1915
https://doi.org/10.1007/s42417-022-00490-3

ORIGINAL PAPER

Prediction of Bearing Fault Effect on the Hydraulic Performances of a Centrifugal Water Pump

Faouzi Omri[1] · Oussema Choura[1] · Lamjed Hadj Taieb[2] · Sami Elaoud[3]

Received: 8 December 2021 / Revised: 25 March 2022 / Accepted: 27 March 2022 / Published online: 13 April 2022

Abstract

Background Bearing faults in centrifugal pumps usually result in periodically fluctuating torque, which leads to flow instabilities, pressure pulsation, excessive heating, and even pump failure.

Purpose This paper presents a theoretical approach for modeling and analyzing the impact of some typical bearing faults on the dynamic characteristics of a monoblock centrifugal pump.

Method The governing equations of the flow are solved by the method of characteristics, while the dynamic parameters of the asynchronous motor are predicted by adopting the *d*-*q* axes theory. Bearing faults are modeled as periodic square-wave pulses injected into the shaft of the pump.

Result The studies of the simulation results show that bearing fault has no significant impact on the pump H-Q curve but it has a large negative effect on the efficiency curve. Additionally, bearing failure in centrifugal pumps can induce head oscillation and flow rate fluctuation.

Conclusion In this work, the influence of bearing anomalies on the performance of centrifugal pumps was analyzed using a numerical method. The model analysis indicated that bearing faults in centrifugal pumps can lead to remarkable performance degradation, severe vibrations, and significant flow instabilities.

Keywords Bearing faults · Centrifugal pump · Induction motor · Time domain signals · Fast Fourier transform · Method of characteristics

Introduction

Centrifugal pumps are the most commonly used devices for energy conversion and fluid transport. Continuous monitoring of pump systems is critical to ensure safe operation, prevent unexpected failures, reduce repair costs and avoid downtime [1]. Bearings are important mechanical components that have major impact on the pump performances. They are properly dimensioned to withstand the hydraulic loads on the impeller while minimizing friction losses. Bearing failures in radial pumps can induce dangerous distresses, namely the following: noise, overheating, high vibration level and a significant drop in performances [2]. In general, the main causes of bearing failures are associated with contamination, corrosion, inadequate lubrication, and misalignment or overloading [3].

Over the years, condition monitoring and fault diagnostics of rolling bearings has been the subject of extensive research [4]. Various methods and techniques have been developed, including vibration signal analysis, infrared

✉ Faouzi Omri
omrifawzi@yahoo.fr

Oussema Choura
oussema.choura@gmail.com

Lamjed Hadj Taieb
l.hadjtaieb@psau.edu.sa

Sami Elaoud
elaoudsa@yahoo.fr

[1] Laboratory of Applied Fluid Mechanics, Process Engineering and Environment, National School of Engineering of Sfax, 3038 Sfax, Tunisia

[2] Mechanical Engineering Department, College of Engineering, Prince Sattam Bin Abdulaziz University, Al-Kharj, Saudi Arabia

[3] Laboratory of Applied Fluid Mechanics, Process Engineering and Environment, National School of Engineering of Sfax, 3038 Sfax, Tunisia

thermography, motor speed and motor current analysis [5]. For radial pumps, bearing anomalies can also be detected by continuously monitoring its operating parameters such as the dynamic pressure, the flow rate, drive power and impeller rotation speed [6].

In the mid-1990s, Greene and Casada [7] investigated pump defect detection methods commonly used in nuclear power plants in the United States. The authors compared these methods with engineering diagnostic programs and practices used in and by other industries. They concluded that vibration spectral analysis is widely accepted as an extremely powerful tool for detecting pump anomalies such as bearing faults, misalignment, unbalance and looseness. Later, Thomson & Orpin [8] proposed a combination of vibration signal analysis and current signal analysis to identify potential problems in induction motor drives. It has been shown that, in electrical drive systems, simultaneous analysing of both electrical and mechanical signals works better in identifying faults and determining their cause. Orhan et al. [9] monitored vibration signals from a relatively large centrifugal pump to investigate the possible defects in ball and roller bearings. The authors used FFT algorithm techniques for data analysis. In this study, it has been found that bearing defects behave in an identical manner independently of the rolling-element type. As noted in the above study, the amplitudes of the high frequencies often decrease when a bearing defect reaches an advanced stage, as the defects become self-peening.

Recently, the use of a combination of two or more techniques to process vibration signal has grown significantly. Wang and Chen [10] proposed an intelligent method for fault diagnosis in a centrifugal pump that includes unbalance and misalignment. The authors used partially linearized neural networks (PNN), rough sets and wavelet transform (WT) techniques to extract fault features from measured vibration signals. They demonstrated that the PNN technique quickly converges in learning and can accurately distinguish fault types in diagnosis based on the probability distributions of symptom parameters. Zhang et al. [11] developed an approach to diagnose bearing faults based on the vibration signals analysis using multi-scale entropy (MSE) and adaptive network fuzzy inference system (ANFIS). Experiments were conducted on electrical motor bearings with three different fault categories. A similar approach was adopted by Farokhzad [12] to diagnose malfunctions in centrifugal pumps. The pump test conditions were healthy, impeller broken, impeller worn, leakage and/or cavitation. The most important features were extracted from vibration signals using the conventional FFT technique. Moreover, Yunlong & Peng [13] introduced a new method based on Empirical Mode Decomposition (EMD) and least square support vector machine (LS–SVM) for vibration signals analysis of a centrifugal pump. The proposed technique has been shown to be effective in extracting non-linear features with non-stationary characteristics when a misalignment fault is considered. In addition, the SVM algorithm was exploited later by Xue et al. [14] to diagnose common faults in a centrifugal pump at an early stage. The pump test conditions were as follows: cavitation, impeller unbalance, and shaft misalignment. It has been shown though practical and experimental test examples that the method is suitable for the analysis of vibration signals and that it is able to correctly identify fault types.

More recently, Altobi et al. [15] have experimentally investigated the performance of the fast Fourier transform (FFT) as a frequency domain analysis tool for identifying specific pump conditions. The FFT technique has proven effective in identifying centrifugal pump conditions that produce stationary signals (i.e., misalignment, imbalance and looseness). However, it is limited in its ability to detect precise significant frequencies of faults generating non-stationary signals (i.e., impeller faults…). A novel technique for the detection of bearing faults has been proposed by Jamadar et al. [16]. The authors successfully developed a theoretical model for numerical calculation of the vibration response parameters of damaged pump bearings. They concluded that the frequency configuration of pump bearing vibration has different components, namely the frequency of rotation of the pump shaft and the frequency of bearing damage. Nasef et al. [2] conducted an experimental study to evaluate the condition of a centrifugal pump and diagnose faults, if any. The study dealt with bearing faults and impeller defects. The following three vibration methods were used: root-mean-square (RMS), time-domain analysis (TDA) and data envelop analysis (DEA). In addition, Gao et al. [17] proposed an improved model to predict the vibration response of hydraulic pipeline system under multiple and various excitations. A numerical approach coupling the method of characteristics (MOC) to the finite element method (FEM) was adopted to solve fluid and pipe/structure equations. The authors found that the fluid pressure signal contains sinusoidal components, with the first three harmonics representing the main energy. Furthermore, it was deduced that pipeline vibration response at the base excitation frequency increases linearly with the excitation amplitude. The condition of a circulation pump with clogged impeller is investigated by Becker et al. [18] using the motor current signature analysis (MCSA) technique. It has been shown that the efficiency of the pump can be reduced by 9–15% compared to the healthy version. The authors also concluded that the largest increase in amplitude at the fault frequency occurs when three and four out of seven channels are clogged.

As an effective tool for detecting bearing anomalies, the acoustic emission method (AE) was successfully applied by Tabatabaei et al. [19] to an experimental case involving defects in an angular contact bearing. The raw acoustic signals are

extracted using AE sensors at different conditions and then decomposed by empirical mode decomposition (EMD). For a similar purpose, Aasi et al. [20] developed an experimental test rig for condition monitoring of angular contact bearing by using an acoustic emission sensor. Time-domain signals from inner and outer ring bearing faults are analysed for different loads, speeds, and sizes. It was found that the clearance, the sixth central moment, the impulse, the kurtosis and the crest factors are suitable characteristics for diagnosis.

Equally important is the research by Bek et al. [21], which deals with vibrations. The authors used the nonlinear stability analysis approach to investigate the effects of inviscid fluid flow on the stability of a damped spring pendulum motion. In addition, Amer et al. [22] studied the combined effect of a viscous liquid and a moving mass on the dynamical motion of a symmetric rigid body around a principal axe. They concluded that in the presence of internal dissipation, the motion of the system eventually approached stationary rotation around the axis of greatest moment of inertia. The importance of their work goes back to their direct applications in the submarine, turbomachinery and gyroscope industries.

Condition monitoring and fault diagnosis of centrifugal pumps have been intensively studied in previous research. Most of the known techniques are based on the vibration signal, the acoustic emission method or the motor current signal analysis. On the other hand, monitoring the bearing condition in turbopumps remains complex and difficult to decipher, due to numerous sources of noise and vibration, such as impeller volute interaction, misalignment and cavitation. In addition, it is worth noting that, for radial pumps, the analysis of hydraulic parameters for detecting bearings anomalies has not been well researched. Therefore, the impact of such defects on the hydraulic performances of a pump were not sufficiently analysed and there are still many unknown issues related to the effect of these anomalies on the efficiency and reliability of centrifugal pumps that remain to be investigated.

The main focus of this research is to develop a simple numerical tool to predict and analyse the effect of some typical bearing faults on the operating parameters of radial pumps. Consequently, this work proposes a new numerical method that can provide useful information dealing with bearing defects and their impact on the hydraulic performance of motor pumps.

Methods

Dynamic Model of the Induction Motor

Most centrifugal pumps are currently manufactured as electric monoblock units. The pump and the induction motor are directly coupled to the same shaft. Therefore, the pump dynamic behaviour depends on its drive motor. In this study, the dynamic modelling of the induction motor is based on the d–q axis theory for electrical machines. This method is well tested and proves to be effective for approximating the motor response in static and transient regimes.

In the stationary reference frame, the three–phase stator voltage equation can be expressed by using the stator resistance (R_s) and the instantaneous stator flux linkage per phase (φ_s) as follows:

$$\begin{bmatrix} v_{s1} \\ v_{s2} \\ v_{s3} \end{bmatrix} = R_s \begin{bmatrix} i_{s1} \\ i_{s2} \\ i_{s3} \end{bmatrix} + \frac{d}{dt} \begin{bmatrix} \varphi_{s1} \\ \varphi_{s2} \\ \varphi_{s2} \end{bmatrix} \tag{1}$$

In a similar way the rotor voltage equation can be formulated using the rotor resistance (R_r) and the instantaneous rotor flux linkage per phase (φ_r) as follows:

$$\begin{bmatrix} 0 \\ 0 \\ 0 \end{bmatrix} = R_r \begin{bmatrix} i_{r1} \\ i_{r2} \\ i_{r3} \end{bmatrix} + \frac{d}{dt} \begin{bmatrix} \varphi_{r1} \\ \varphi_{r2} \\ \varphi_{r2} \end{bmatrix} \tag{2}$$

The d–q model consists of converting the three windings of the induction motor into only two windings without affecting the behaviour of the machine. As it is shown in Fig. 1, For any arbitrary value of θ, the transformation of the stator and the rotor variables from the three phases stationary coordinates (x_1, x_2, x_3) to the (d, q) rotating coordinates is carried out through Park transformation described as follows [23]:

$$\begin{bmatrix} x_d \\ x_q \end{bmatrix} = P(\theta) \begin{bmatrix} x_1 \\ x_2 \\ x_3 \end{bmatrix} \tag{3}$$

where,

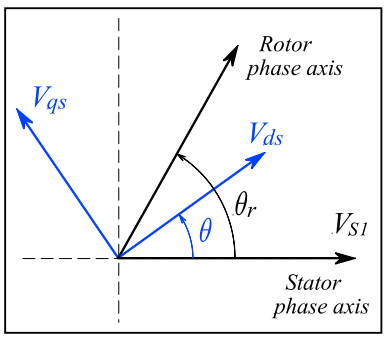

Fig. 1 Stator voltage space vector in *d–q* plane

$$P(\theta) = \sqrt{\frac{2}{3}}\begin{bmatrix} \cos(\theta) & \cos(\theta - 2\pi/3) & \cos(\theta + 2\pi/3) \\ -\sin(\theta) & -\sin(\theta - 2\pi/3) & -\sin(\theta + 2\pi/3) \end{bmatrix}, \tag{4}$$

in which θ is the angle between the real axis of the stator and the real axis of the reference system rotating with the rotor.

The stator voltage equations in the (d, q) planes are expressed as follows:

$$\begin{bmatrix} v_{ds} \\ v_{qs} \end{bmatrix} = P(\theta)\begin{bmatrix} v_{s1} \\ v_{s2} \\ v_{s3} \end{bmatrix} \tag{5}$$

In the rotating frame of reference (d, q), the induction motor current equations for the stator and rotor windings, after transformations, can be written as [24] follows:

$$\begin{bmatrix} v_{ds} \\ v_{qs} \end{bmatrix} = R_s\begin{bmatrix} i_{ds} \\ i_{qs} \end{bmatrix} + L_s\frac{d}{dt}\begin{bmatrix} i_{ds} \\ i_{qs} \end{bmatrix} + M\frac{d}{dt}\begin{bmatrix} i_{dr} \\ i_{qr} \end{bmatrix} + w_s\begin{bmatrix} -L_s i_{qs} - Mi_{qr} \\ L_s i_{ds} + Mi_{dr} \end{bmatrix} \tag{6}$$

$$\begin{bmatrix} 0 \\ 0 \end{bmatrix} = R_r\begin{bmatrix} i_{dr} \\ i_{qr} \end{bmatrix} + L_r\frac{d}{dt}\begin{bmatrix} i_{dr} \\ i_{qr} \end{bmatrix} + M\frac{d}{dt}\begin{bmatrix} i_{ds} \\ i_{qs} \end{bmatrix} + w_r\begin{bmatrix} -L_r i_{qr} - Mi_{qs} \\ L_r i_{dr} + Mi_{ds} \end{bmatrix} \tag{7}$$

where, i_{ds}, i_{qs} are the stator direct-axis and quadrature-axis currents, i_{dr}, i_{qr} are the rotor direct-axis and quadrature-axis currents, R_s, R_r are the electrical resistances of the stator and rotor, L_s, L_r are the cyclic inductances of the stator and rotor, M is the mutual cyclic stator–rotor inductance.

The stator and rotor pulsation are given as follows:

$$w_r = (1 - g)\frac{w_s}{p}, w_s = \frac{d\theta}{dt} \tag{8}$$

where g is the sliding coefficient and p is the pole number of the motor.

The stator current is expressed as follows:

$$i_s = \sqrt{\frac{2}{3}}\left(i_{ds}\cos\left(w_s t\right) - i_{qs}\sin\left(w_s t\right)\right) \tag{9}$$

The electromagnetic torque developed by the motor is given as follows:

$$T_{em} = p.M\left(i_{dr}i_{qs} - i_{qr}i_{ds}\right) \tag{10}$$

The motor characteristics are calculated by a simple integration of the previous Eqs. (6) and (7) taking into account the load torque of the pump.

Bearing Faults Modelling

In centrifugal pumps, bearings are used to support and guide rotating parts (motion transmission), and reduce friction between the components rotating relative to one another. They are dimensioned to support radial and axial loads generated by the impeller. When the balls pass the point of failure of the bearing an additional load moment is applied to the pump shaft. This affects the parameters of the bearing structure and the speed of motor for a short period of time. The length of that period of time depends on the size of the fault area [25]. In this study, the periodic rectangular pulse shown in Fig. 2 is considered to simulate the bearing fault torque. The pulse width,τ, denotes the fault impact duration in the fault period,T, and Γ indicates the fault amplitude.

The Fourier decomposition of the bearing fault signal can be written in terms of the period T as follows:

$$T_{\text{Fault}} = a_0 + \sum_1^{\infty}\left(a_n\cos\left(\frac{2\pi n}{T}t\right) + b_n\sin\left(\frac{2\pi n}{T}t\right)\right) \tag{11}$$

In the case of Fig. 2, the Fourier series coefficients are expressed as follows:

$$a_0 = \Gamma\frac{\tau}{T} \tag{12}$$

$$a_n = \frac{2\Gamma}{\pi n}\sin\left(n\pi\frac{\tau}{T}\right) \tag{13}$$

Because of the parity of the signal T_{Fault}, the values of the coefficients b_n were set to zero. Thus, the bearing fault load torque can finally be described as follows:

$$T_{\text{Fault}} = \Gamma\frac{\tau}{T} + \sum_1^{\infty}\frac{2\Gamma}{\pi n}\sin\left(n\pi\frac{\tau}{T}t\right) \tag{14}$$

The bearing fault frequency ($f = 1/T$) is a function of the motor speed and the bearing geometry. It can be calculated using equations given in Table 1 as follows:

in which D is the pitch diameter, d is the ball diameter, n_r is the number of rolling elements, f_N is the impeller rotation frequency and $\varnothing$ is the ball contact angle.

Equations of Motion

The radial pump is directly coupled to a three-phase asynchronous motor with the same shaft. To overcome the load torque opposed by the rotating parts of the pump and the

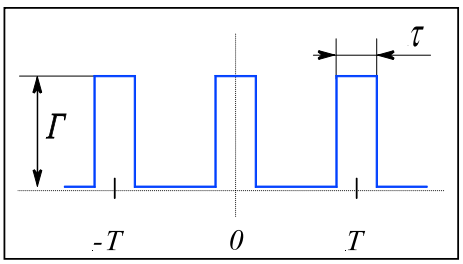

Fig. 2 Time domain diagram of bearing fault load torque

Table1 Fault frequency expressions and value for bearing SKF 6205 (N=2890 rpm)

Bearing fault types	Frequency expressions	
Inner race frequency	$f_{\mathrm{IR}} = \frac{n_r}{2} f_N \left(1 + \frac{d}{D}\cos\varnothing\right) = 260.82\mathrm{Hz}$	(15)
Outer race fault frequency	$f_{\mathrm{OR}} = \frac{n_r}{2} f_N \left(1 - \frac{d}{D} cos\varnothing\right) = 172.66\mathrm{Hz}$	(16)
Fundamental train frequency	$f_{\mathrm{FT}} = \frac{1}{2} f_N \left(1 - \frac{d}{D} cos\varnothing\right) = 19.86\mathrm{Hz}$	(17)
Ball spin frequency	$f_{\mathrm{BS}} = \frac{D}{2d} f_N \left(1 - \left(\frac{d}{D} cos\varnothing\right)^2\right) = 112.37\ \mathrm{Hz}$	(18)

friction of the moving fluid, the motor develops an electromagnetic torque that can be expressed as follows:

$$T_{em} = \left(I_M + I_P\right)\frac{d\Omega}{dt} + T_{\mathrm{Load}}, \quad (19)$$

in which I_M is the inertia of the motor, I_P is the inertia of the impeller including the rotating water inertia and T_{load} is the load torque of the centrifugal pump.

When bearing fault occurs, the load torque equation is written as follows:

$$T_{\mathrm{Load}} = T_r + T_{\mathrm{fault}}, \quad (20)$$

where T_r is the resistant torque generated by the hydrodynamic and mechanical components. The resistant torque depends on the impeller angular speed Ω and the fluid flow rate Q [26]:

$$T_r = k_1\Omega^2 + k_2\Omega Q - k_3 Q^2 \quad (21)$$

The hydrodynamic torque coefficients k_1, k_2 and k_3 are determined from the characteristic curves of the pump in steady-state.

The substitution of Eq. 14 and Eq. 21 in Eq. 20 yields the following:

$$T_{\mathrm{Load}} = \Gamma\frac{\tau}{T} + \sum_1^{\infty}\left(\frac{2\Gamma}{\pi n}\sin\left(n\pi\frac{\tau}{T}t\right)\right) + k_1\Omega^2 + k_2\Omega Q - k_3 Q^2 \quad (22)$$

Model of the flow

The flow in the centrifugal impeller is modeled using the one-dimensional approach described by Thanapandi and Prasad [27], Chalghoum et al. [28] and Omri et al. [29]. The basic continuity and motion equations, in a rotating reference frame associated with the impeller, are simplified as follows:

$$\frac{\partial H}{\partial t} + \frac{C^2}{gA}\frac{\partial Q}{\partial x} = 0 \quad (23)$$

$$\frac{1}{A}\frac{\partial Q}{\partial t} + g\frac{\partial H}{\partial x} + \lambda\frac{Q|Q|}{2DA^2} - \delta r\Omega^2 = 0, \quad (24)$$

in which t is time, x is the space distance along the impeller passage,A is the impeller cross-sectional area, Q is the flow rate, H is the pressure head, C is the pressure wave velocity, D is the hydraulic diameter of the section A, λ is the friction coefficient and Ω is the impeller angular velocity.

In the momentum equation, the source term $r\Omega^2$ represents the effect of the centrifugal force created by the rotation of the impeller. The coefficient δ in eq. (24) mimics the impeller slip factor that depends on the vanes number, the blade exit angle and the pump flow rate.

It is worth noting that the continuity equation (eq. 23) is derived from the mass conservation law taking into consideration the mass unsteadiness due to the compressibility of the moving fluid and the elasticity of the passage material [27].

It is also to note that, for flows in a stationary frame associated with the volute and pipes, the effect of centrifugal force is disregarded from eq. (24).

Numerical Method

In order to analyse the pump characteristics in the case of bearing faults, the unsteady flow equations are solved numerically using the method of characteristics (MOC). The method consists of reducing the simplified equation of motion and continuity (Eqs. 23 and 24) to a system of ordinary differential equations (Eqs. 25 and 26) valid only along characteristic lines C^+ and C^- as shown in Fig. 3.

$$C^+\begin{cases}\frac{gA}{C}dH + dQ + gJAdt - \delta r\Omega^2 Adt = 0\\ \frac{dx}{dt} = V + C\end{cases} \quad (25)$$

$$C^-\begin{cases}-\frac{gA}{C}dH + dQ + gJAdt - \delta r\Omega^2 Adt = 0\\ \frac{dx}{dt} = V - C\end{cases} \quad (26)$$

The friction head loss by unit of the impeller passage length is expressed as follows:

$$J = \lambda\frac{Q|Q|}{2DA^2} \quad (27)$$

To simplify the numerical calculations and to reduce the computational efforts, the impeller geometry is simplified

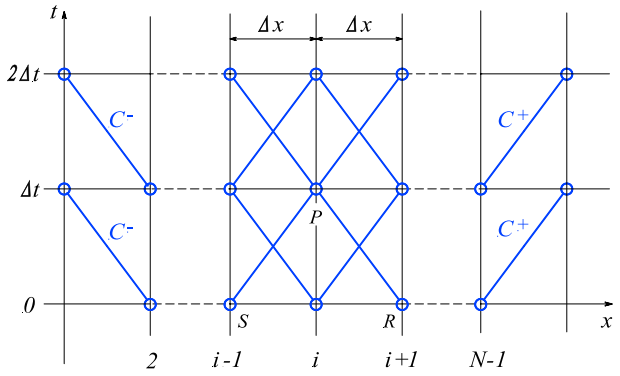

Fig. 3 Characteristic lines and computational grid

into two-dimensional straight-blades (Fig. 4). Furthermore, it is assumed that the blade height is constant along the meridional flow path.

The flow through the impeller is calculated according to a one-dimensional discretization approach under consideration of the MOC convergence condition. Assuming a time interval Δt (discretization step within the time axis), the length of flow path L (see Fig. 4) is divided into N equal sections ($N = L/\Delta x$). The calculation process starts at $t = t_0$ with known steady-state conditions in all N sections of the grid (Fig. 3). Integration of equations Eq. (25) and Eq. (26) along the characteristic lines results in a set of finite-difference equations as follows:

$$C^{+}: Q_{Pi} - Q_{i-1} + \frac{gA_{i-1}}{C}(H_{Pi} - H_{i-1}) + A_{i-1}(J_{i-1} - r_{i-1}\delta\Omega^2)\Delta t = 0 \tag{28}$$

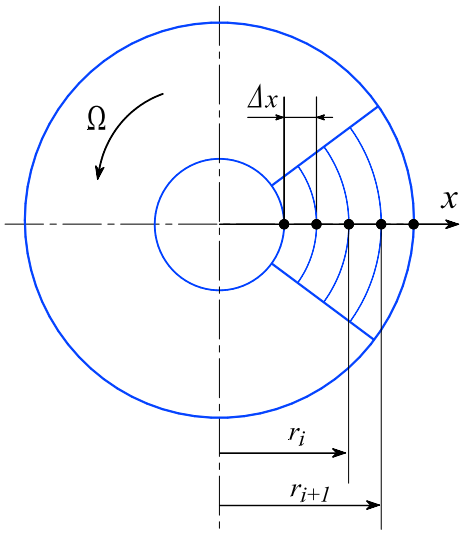

Fig. 4 Simplified impeller geometry and space grid

$$C^{-}: Q_{Pi} - Q_{i+1} - \frac{gA_{i+1}}{C}(H_{Pi} - H_{i+1}) + A_{i+1}(j_{i+1} - r_{i+1}\delta\Omega^2)\Delta t = 0 \tag{29}$$

Equations (28) and (29) are solved simultaneously, for each time step Δt, to calculate the unknowns H_{Pi} and Q_{Pi} at each grid point P_i. Similarly, the flows within the casing volute and the pipes were analysed following the same process without consideration of the centrifugal force term. Since the dynamic head and discharge of the pump depend on the impeller speed, Eqs. (6) and (7) are solved simultaneously with Eq. (22) for each time step Δt. In this way, the hydraulic variables of the pump, the motor speed and the rate of change of the motor torque under bearing defects can be determined.

Result and discussion

The numerical model developed above is applied to analyse the hydraulic characteristics of the centrifugal pump under bearing fault conditions.

Model Validation

The experimental studies of Zhou et al. [30] were used to validate the proposed model. The test pump was a single stage, volute type with vertical shaft and driven by a three-phase asynchronous motor (7500 W). The length of the suction pipe and discharge pipe are 1.2 m and 3.2 m, respectively. The main parameters of the tested pump are summarized in Table 2.

To follow the actual operating conditions, the pump specifications listed in Table 2 were introduced to the numerical code. At this stage, a series of simulations were carried out under healthy conditions. The pump performances curves were determined considering different flow rate. A comparison between simulated and measured results is presented in Fig. 5. It can be seen that the simulated performances curves agree well with experimental data. A small shift between experiments and simulations can be observed in Fig. 5. This can be caused by the approximation of the hydraulic losses

Table 2 Main parameters of the radial pump

Description	Parameter	value
Design flow rate (m^3/h)	Q	40
Pressure head (m)	H	30
Impeller speed (rpm)	N	2850
Impeller outlet diameter (mm)	D_2	168
Impeller blade exit angle (°)	β_2	12
Impeller outer width (mm)	b_2	11
Impeller blade number (−)	Z	6

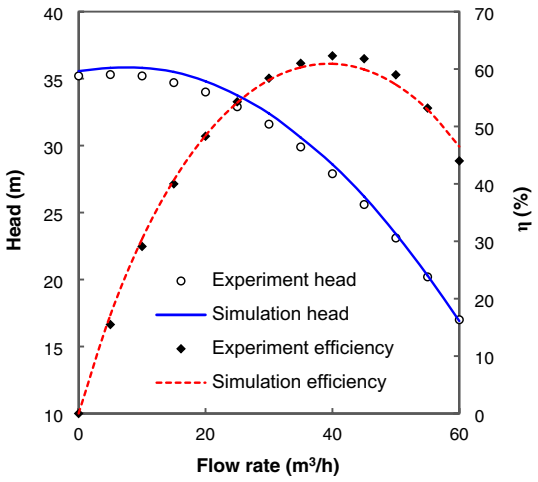

Fig. 5 Comparison of experimental [30] and numerical pump external characteristics

in the pump and the simplification of the impeller geometry (negligence of the curvature).

Analysis of the pump performance under bearing defects

Numerical analysis of the pump system response to bearing failure is performed when the pump is operating at its rated speed. The effect of the bearing fault was simulated as a small periodic rectangular pulse with $\tau = 0.2T$ injected into the load torque. As shown in Table 3, three typical bearing defects were considered in this study which are fundamental train defect (Case.1), ball spin defect (Case.2) and outer race defect (Case.3).

A numerical study of the effect of the bearing faults on the steady-state characteristics of the pump from cases1 and 2 are shown in Fig. 6. A small drop of 0.5 m can be seen in the H–Q curves between the healthy and faulty cases. This effect decreases with the increase of the discharge flow rate. However, the influence of the bearing defects on the efficiency curves is remarkable. Near the best operating point ($Q = 40$ m^3/h), the efficiency drops from 60.91% to 52.3% and thus the power consumed by the pump increases considerably. Since the same amplitude of the faulty torque is applied in cases 1 and 2, it is important to recognize that the bearing faults have approximately the same effect on the steady-state performance of the pump in both cases. It can be seen from Fig. 6 that the fault frequency has no significant effect on the pump's steady-state characteristics.

Table 3 Test condition for bearing faults

Case no	Fault type	Frequency (Hz)	Average fault torque (Nm)
Case.1	Fundamental train (FT)	f FT = 19.86	3.129
Case.2	Ball spin (BS)	f BS = 112.37	3.129
Case.3	Outer race (OR)	f OR = 172.66	3.129

Hydraulic signal analysis under bearing defects

In all cases, the average flow rate is 39.767 m^3/ h when the pump is running at 2869.5 rpm and the average head is 28.459 m. The calculated results of the hydraulic signals are presented in time and frequency domains. The sampling rate is 10000, while the number of collected data is 5000. In the time domain representation, the DC component is abstracted from the original signal. Then, the fast Fourier transform (FFT) algorithm is applied to convert the signals to the frequency domain.

Fundamental train defect analysis

The time history of the calculated head developed by the pump in the event of a fault in the basic bearing train is shown in Fig. 7a. A regular low-frequency waveform with an amplitude of 0.5 m is observed. This can lead to serious vibration in the discharge pipe. In Fig. 7b, the fundamental train defect frequency $f_{FT} = 19.86$ Hz and its multiples are clearly visible in the head spectrum. The amplitude of the harmonics decreases with increasing frequency, while the maximum peak value corresponds to the fundamental frequency of the fault. Figure 8a, on the other hand, shows the time signals of the pump flow rate with bearing fundamental train defect. A small periodic fluctuation at the fault frequency (f_{FT}) is clearly seen in time domain representation. The FFT analysis of the flow rate signal is shown in Fig. 8b. The frequency of the bearing fault and its harmonics can be

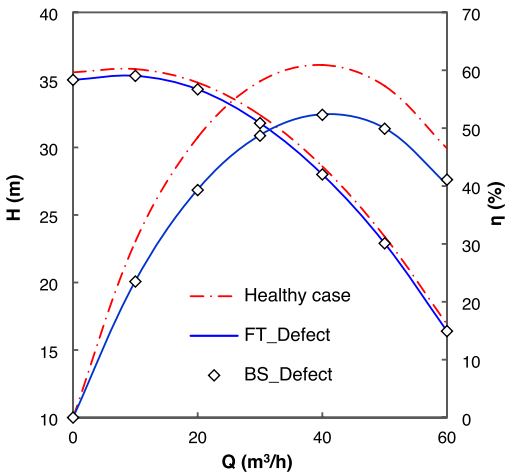

Fig. 6 Effect of the bearing faults on the pump performance curves

seen in the flow spectrum, which clearly shows the relationship between the torque of the bearing fault and its effects on the hydraulic parameters of the pump. This confirms the theoretical approach of the flow modeling and the robustness of the motor torque model in the presence of bearing defects.

Ball spin defect analysis

The time signal of the simulated pump head with a bearing ball spin defect is shown in Fig. 9a. The head oscillations are relatively small and faster than in case.1. As can be seen in Fig. 9b, the head spectrum peaks at $f_{BS} = 112.37$ Hz and its multiples confirm the effects of the bearing damage on the pump pressure. The numerically determined pump flow rate time signal is plotted in Fig. 10a. The flow rate signal oscillates at twice the frequency of the ball rotation fault ($2xf_{BS}$) with regular amplitude. In the spectrum of the flow rate shown in Fig. 10b, the first harmonic is dominant, while the fundamental is smoothed probably due to the inertia effect.

Outer race defect analysis

The transient performances of the pump when the outer bearing ring is defective are shown in Fig. 11 and Fig. 12. An irregularly oscillating head with amplitude of 0.05 m is clearly visible in the time domain representation (Fig. 11a). Compared to case.1 and case.2, a significant decrease in the amplitude of the head oscillation can be seen. The signature of the outer race fault is clearly shown in the FFT of the pressure head (Fig. 11b). The fundamental frequency (f_{OR}) is the strongest, the third and fourth harmonics exist but the second ($3xf_{OR}$) is smoothed. As can be seen in Fig. 12a, the

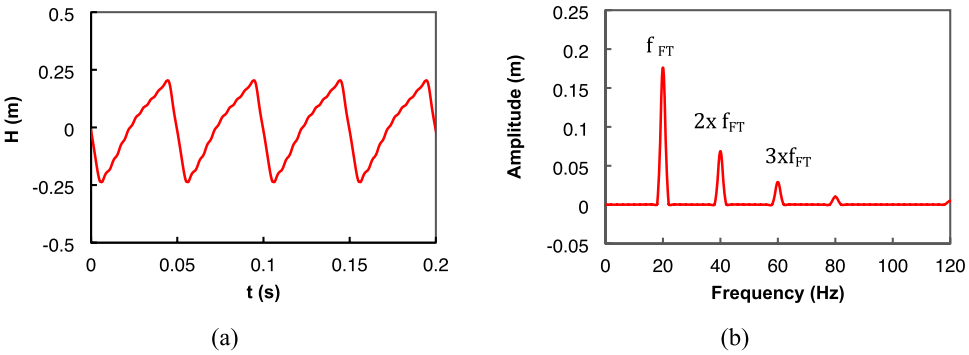

(a) (b)

Fig. 7 Simulation of fluid pressure signals under fundamental train defect: **a** pump head signal in time domain and **b** pump head signal in frequency domain

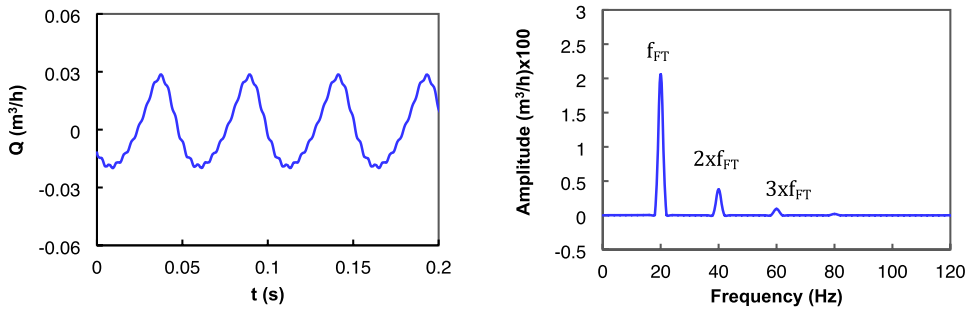

(a) (b)

Fig. 8 Simulation of fluid flow rate signals under fundamental train defect: **a** flow rate signal in time domain and **b** flow rate signal in frequency domain

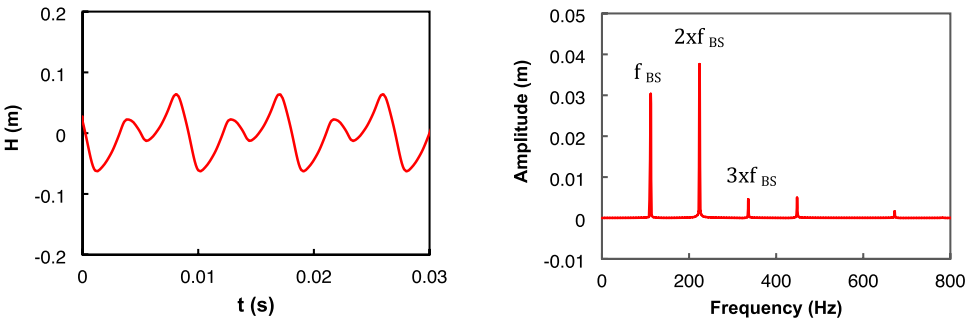

(a) (b)

Fig. 9 Simulation of fluid pressure signals under ball spin defect: **a** pressure signal in time domain and **b** pressure signal in frequency domain

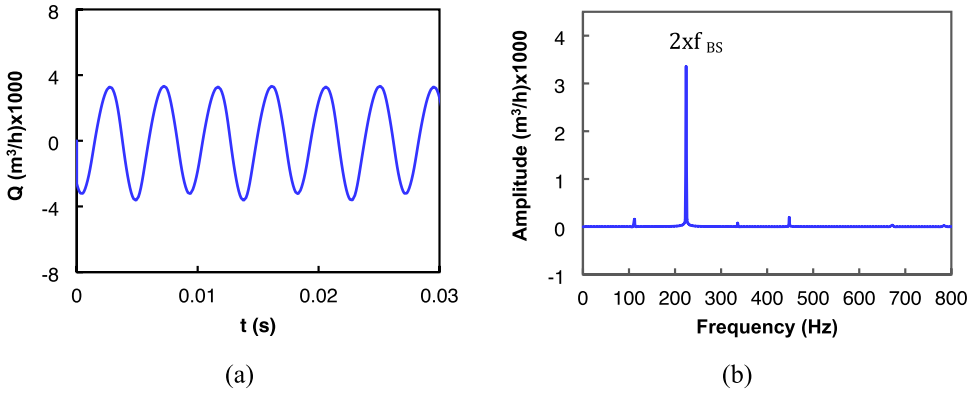

Fig. 10 Simulation of fluid flow rate signals under ball spin defect: **a** flow rate signal in time domain and **b** flow rate signal in frequency domain

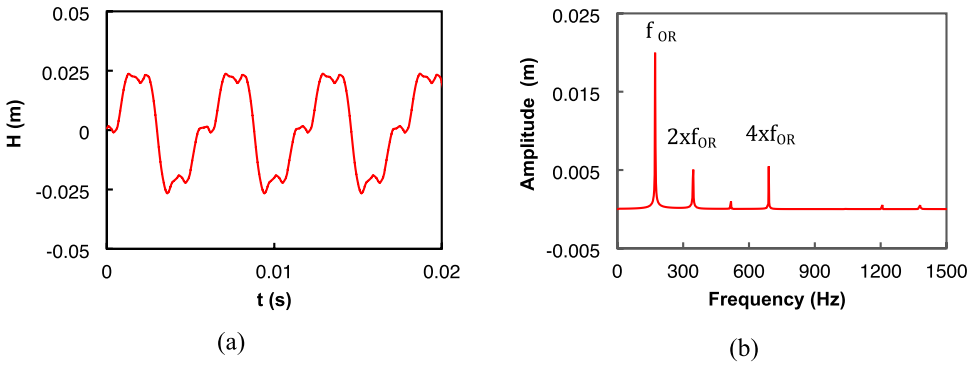

Fig. 11 Simulation of fluid pressure signals under outer race defect: **a** pressure signal in time domain and **b** pressure signal in frequency domain

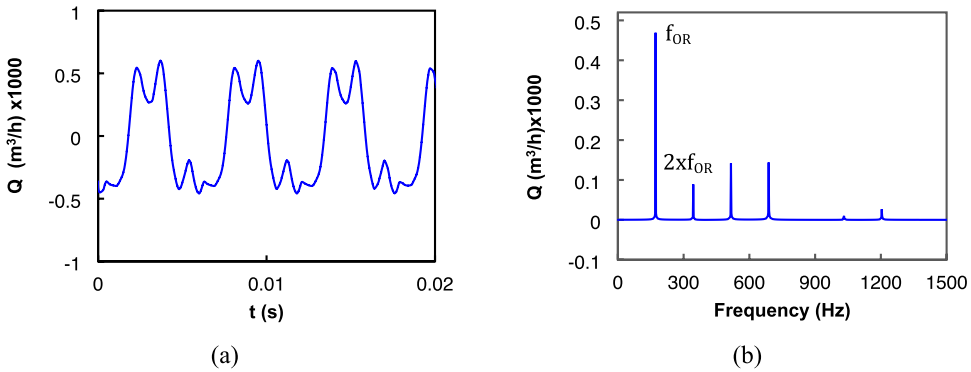

Fig. 12 Simulation of fluid flow rate signals under Outer race defect: **a** flow rate signal in time domain and **b** flow rate signal in frequency domain

flow rate signal oscillates with irregular amplitude at the fault frequency (f_{OR}). In Fig. 12b, the fundamental (f_{OR}) and its harmonic appear in the spectrum of the flow rate. Beyond the third harmonic, no important information can be detected in the FFT of the flow rate.

Influence of bearing fault frequency

The analysis of the effect of frequency on the fluctuation of pump flow at different fault amplitudes is shown in Fig. 13. In the low-frequency range, the bearing anomalies produce strong oscillations in the signals for head and flow. From Fig. 13a, it can be seen that fluctuation level in head signal decreases with increasing frequency. Furthermore, in Fig. 13b, the oscillation of flow rate becomes insignificant beyond the frequency of 100 Hz. This could be due to the effect of flow inertia, especially when the pump is running at high flow rate.

Conclusion

In this work, the influence of bearing anomalies on the performance of centrifugal pumps was analysed using a numerical method. Three typical bearing faults have been considered: fundamental train defect, ball spin defect and outer race defect. The studies of the simulation results show the following conclusions:

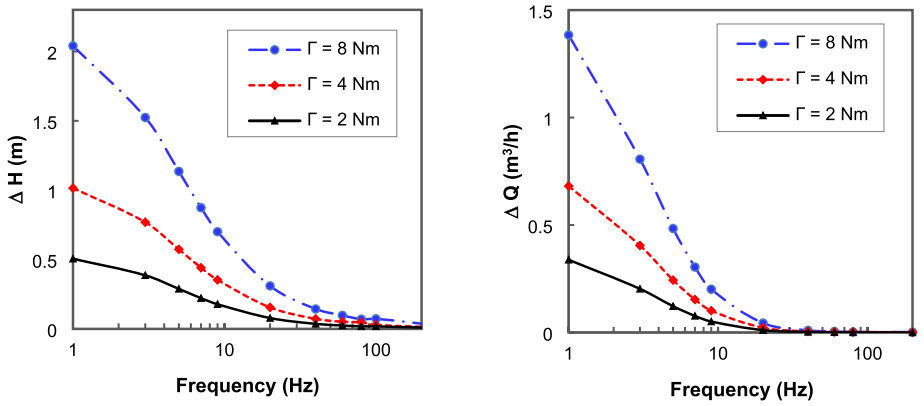

(a) (b)

Fig. 13 Peak to peak value of (**a**) pressure fluctuation and **b** flow rate fluctuation for different bearing fault frequency

- From the steady-state performance analysis, the bearing fault has no significant impact in the pump H-Q curve but a large negative effect can be found in the efficiency curve.
- Bearing failure in centrifugal pumps leads not only to a remarkable efficiency degradation but also to an oscillating pressure head and fluctuating flow rate.
- The frequency of the bearing failure and its harmonics can be detected in the FFT plot in both the pressure head and flow rate signals.
- The amplitude of the fluctuations in the time domain is more significant in the evolution of the pressure head than in the flow rate.
- The inertia of the flow reduces the fluctuations in pressure head and flow rate, especially for high-frequency bearing defects.

With reasonable accuracy and easy implementation, the proposed method helps engineers and researchers to predict the behaviour of radial pumps under bearing fault conditions.

Funding The authors did not receive support from any organization for the submitted work.

Declarations

Conflict of Interest On behalf of all authors, the corresponding author states that there is no conflict of interest.

References

1. Sakthivel NR, Nair BB, Sugumaran V (2012) Soft computing approach to fault diagnosis of centrifugal pump. Appl Soft Comput 12(5):1574–1581. https://doi.org/10.1016/j.asoc.2011.12.009
2. Nasef MH, Hashim MA, Osman OO (2020) Experimental investigation of fault diagnosis for centrifugal pump based on vibration signals. Int J Adv Sci Technol 29(01):889–898
3. Leite VCMN, da Silva JGB, Torres GL, Veloso GFC, da Silva LEB, Bonaldi EL, de Oliveira LEDL (2017) Bearing fault detection in induction machine using squared envelope analysis of stator current. Bearing technology. InTech, London, UK. https://doi.org/10.5772/67145
4. Janjarasjitt S, Ocak HASAN, Loparo KA (2008) Bearing condition diagnosis and prognosis using applied nonlinear dynamical analysis of machine vibration signal. J Sound Vib 317(1–2):112–126. https://doi.org/10.1016/j.jsv.2008.02.051
5. Cococcioni M, Lazzerini B, Volpi SL (2012) Robust diagnosis of rolling element bearings based on classification techniques. IEEE Trans Industr Inf 9(4):2256–2263
6. Mohanty AR, Pradhan PK, Mahalik NP, Dastidar SG (2012) Fault detection in a centrifugal pump using vibration and motor current signature analysis. Int J Autom Control 6(3–4):261–276
7. Greene RH, Casada DA, Ayers CW (1995) Detection of pump degradation (No. NUREG/CR--6089). Nuclear Regulatory Commission.
8. Thomson WT, Orpin P (2002) Current and vibration monitoring for fault diagnosis and root cause analysis of induction motor drives. In: Proceedings of the 31st Turbomachinery Symposium, Texas A&M University. Turbomachinery Laboratories.
9. Orhan S, Aktürk N, Celik V (2006) Vibration monitoring for defect diagnosis of rolling element bearings as a predictive maintenance tool: comprehensive case studies. NDT E Int 39(4):293–298. https://doi.org/10.1016/j.ndteint.2005.08.008
10. Wang H, Chen P (2009) Intelligent diagnosis method for a centrifugal pump using features of vibration signals. Neural Comput Appl 18(4):397–405. https://doi.org/10.1007/s00521-008-0192-4
11. Zhang L, Xiong G, Liu H, Zou H, Guo W (2010) Bearing fault diagnosis using multi-scale entropy and adaptive neuro-fuzzy inference. Expert Syst Appl 37(8):6077–6085. https://doi.org/10.1016/j.eswa.2010.02.118
12. Farokhzad S (2013) Vibration based fault detection of centrifugal pump by fast fourier transform and adaptive neuro-fuzzy inference system. J Mech Eng Technol 1(3):82–87
13. Yunlong Z, Peng Z (2012) Vibration fault diagnosis method of centrifugal pump based on EMD complexity feature and least square support vector machine. Energy Procedia 17:939–945. https://doi.org/10.1016/j.egypro.2012.02.191
14. Xue H, Li Z, Wang H, Chen P (2014) Intelligent diagnosis method for centrifugal pump system using vibration signal and support vector machine. Shock Vib. https://doi.org/10.1155/2014/407570
15. ALTobi MAS, Bevan G, Wallace P, Harrison D, Ramachandran KP (2018) Centrifugal pump condition monitoring and diagnosis using frequency domain analysis. In: International Conference on

Condition Monitoring of Machinery in Non-Stationary Operation, pp 122–131, Springer, Cham. https://doi.org/10.1007/978-3-030-11220-2_13
16. Jamadar IM, Bellary SAI, Kanai RA, Alrobaian AA (2019) Model-based condition monitoring for the detection of failure of a ball bearing in a centrifugal pump. J Fail Anal Prev 19(6):1556–1568. https://doi.org/10.1007/s11668-019-00792-x
17. Gao P, Qu H, Zhang Y, Yu T, Zhai J (2020) Experimental and numerical vibration analysis of hydraulic pipeline system under multiexcitations. Shock Vib. https://doi.org/10.1155/2020/3598374
18. Becker V, Schwamm T, Urschel S, Antonino-Daviu JA (2020) Fault investigation of circulation pumps to detect impeller clogging. Appl Sci 10(21):7550. https://doi.org/10.3390/app10217550
19. Tabatabaei R, Aasi A, Jafari SM (2020) Experimental investigation of the diagnosis of angular contact ball bearings using acoustic emission method and empirical mode decomposition. Advn Tribol 2020:1–14. https://doi.org/10.1155/2020/8231752
20. Aasi A, Tabatabaei R, Aasi E, Jafari SM (2021) Experimental investigation on time-domain features in the diagnosis of rolling element bearings by acoustic emission. J Vib Control. https://doi.org/10.1177/10775463211016130
21. Bek MA, Amer TS, Sirwah MA, Awrejcewicz J, Arab AA (2020) The vibrational motion of a spring pendulum in a fluid flow. Results Phys 19:103465
22. Amer WS, Farag AM, Abady IM (2021) Asymptotic analysis and numerical solutions for the rigid body containing a viscous liquid in cavity in the presence of gyrostatic moment. Arch Appl Mech 91(9):3889–3902
23. Lee RJ, Pillay P, Harley RG (1984) D, Q reference frames for the simulation of induction motors. Electric Power Syst Res 8(1):15–26
24. Baghli L (2015) Modélisation et commande de la machine asynchrone. Les Éditions du Net, Saint-Ouen
25. Cheng G, Qiu C, Wu X, Ma J (2016) Research on the speed signature of induction motor bearing fault. In: Proceedings of the 2015 International Conference on Electrical and Information Technologies for Rail Transportation. Springer, Berlin Heidelberg. pp. 19–26. https://doi.org/10.1007/978-3-662-49367-0_3
26. Frelin M (2002) Coups de bélier. Les Tech l'Ingénieur BM 4(176):1–27
27. Thanapandi P, Prasad R (1995) Centrifugal pump transient characteristics and analysis using the method of characteristics. Int J Mech Sci 37(1):77–89
28. Chalghoum I, Elaoud S, Akrout M, Taieb EH (2016) Transient behavior of a centrifugal pump during starting period. Appl Acoust 109:82–89. https://doi.org/10.1016/j.apacoust.2016.02.007
29. Omri F, Hadj Taieb L, Elaoud S (2021) Numerical study on the transient behavior of a radial pump during starting time. AQUA-Water Infrastruct Ecosyst Soc 70(3):257–273. https://doi.org/10.2166/aqua.2021.136
30. Zhou L, Shi W, Wu S (2013) Performance optimization in a centrifugal pump impeller by orthogonal experiment and numerical simulation. Adv Mech Eng 5:385809. https://doi.org/10.1155/2013/385809